E3S Web of Conferences **22**, 00102 (2017) DOI: 10.1051/e3sconf/20172200102
ASEE17

Thermodynamic analysis of a combined-cycle solar thermal power plant with manganese oxide-based thermochemical energy storage

Qi Lei[1], *Roman* Bader[1], *Peter* Kreider[1], *Keith* Lovegrove[1], and *Wojciech* Lipiński[1,*]

[1]The Australian National University, Research School of Engineering, Canberra, ACT, 2601, Australia
[2]IT Power, Canberra, ACT, 2612, Australia

Abstract. We explore the thermodynamic efficiency of a solar-driven combined cycle power system with manganese oxide-based thermochemical energy storage system. Manganese oxide particles are reduced during the day in an oxygen-lean atmosphere obtained with a fluidized-bed reactor at temperatures in the range of 750–1600°C using concentrated solar energy. Reduced hot particles are stored and re-oxidized during night-time to achieve continuous power plant operation. The steady-state mass and energy conservation equations are solved for all system components to calculate the thermodynamic properties and mass flow rates at all state points in the system, taking into account component irreversibilities. The net power block and overall solar-to-electric energy conversion efficiencies, and the required storage volumes for solids and gases in the storage system are predicted. Preliminary results for a system with 100 MW nominal solar power input at a solar concentration ratio of 3000, designed for constant round-the-clock operation with 8 hours of on-sun and 16 hours of off-sun operation and with manganese oxide particles cycled between 750 and 1600°C yield a net power block efficiency of 60.0% and an overall energy conversion efficiency of 41.3%. Required storage tank sizes for the solids are estimated to be approx. 5–6 times smaller than those of state-of-the-art molten salt systems.

1 Introduction

Concentrating solar power (CSP) technologies offer the major benefit of enabling inexpensive thermal energy storage, which allows CSP plants to operate round-the-clock as well as on-demand. Hence, CSP systems are expected to play a central role in future sustainable power systems, particularly in the earth's sunbelt [1]. In this study, we explore the theoretical efficiencies achievable with a solar-driven combined cycle power plant, including a topping Brayton and a bottoming Rankine power cycle, with high-temperature thermochemical energy storage. In combined Brayton-Rankine power cycles, the benefit of high turbine entrance temperatures of gas turbines (> 1000°C [2]) is combined with the

* Corresponding author: wojciech.lipinski@anu.edu.au

high thermal efficiencies of steam Rankine cycles at intermediate operating temperatures, to maximize the operating temperature window and hence the thermal efficiency of the power system. Consequently, combined Brayton-Rankine power cycles are the most efficient commercial power conversion technology to date, with thermal efficiencies approaching 65% [3, 4].

MnO_x is considered as a potential thermochemical energy storage material, due to its suitable reaction temperature range, high storage density, and low cost [5]. In practice, doping of MnO_x with other metals may be required to improve potential issues with pure MnO_x, such as sintering at high temperatures and limited reaction kinetics. However, MnO_x is chosen here as a model material to develop a framework and reference for the assessment of future advanced material compositions. The reversible reduction and oxidation of MnO_x between Mn_2O_3 and MnO occurs via the steps:

$$MnO_2 \leftrightarrow Mn_2O_3 \leftrightarrow \alpha\text{-}Mn_3O_4 \leftrightarrow \beta\text{-}Mn_3O_4 \leftrightarrow MnO \quad (1)$$

The temperatures at which these transitions occur depend on the oxygen partial pressure in the gaseous environment. The Gibbs free energy minimization method has been applied, using the FactSage software [6], to calculate the transition temperatures listed in Table 1. The results show that the required temperatures for the forward (reduction) reaction steps decrease with decreasing oxygen partial pressure in the gas phase, while for the backward (oxidation) reaction steps the opposite applies. Reduction in N_2 gives access to the Mn_3O_4/MnO transition below the slagging temperature. This transition involves a high enthalpy of reaction, and hence strongly increases the mass-specific storage capacity of the solids.

Table 1. Approximate transition temperatures for the redox steps shown in Eq. (1) and associated enthalpy changes.

Substance	$T_{transition}$ (°C)			Δh (kJ kg^{-1})
	N_2	Air	O_2	
Mn_2O_3/α-Mn_3O_4	700	870	963	214
α-Mn_3O_4 /β-Mn_3O_4	1173	1173	1174	80
β-Mn_3O_4 /MnO	1450	1580	1580	897
Slagging	1625	1580	1580	-

The storage system can be operated with any two reversible MnO_x redox pairs in Eq. (1). For example, with the redox pair Mn_2O_3/MnO, operated over the temperature range 750–1600°C, the thermochemical storage process is described by:

Reduction:

$$Mn_2O_3(750^\circ C) \rightarrow 2MnO(1600^\circ C) + 1/2O_2(1600^\circ C); \quad \Delta\bar{h}^\circ = 304.7 \text{ kJ mol}^{-1} \quad (2)$$

Oxidation:

$$2MnO(1600^\circ C) + 1/2O_2(1600^\circ C) \rightarrow Mn_2O_3(750^\circ C); \quad \Delta\bar{h}^\circ = -304.7 \text{ kJ mol}^{-1} \quad (3)$$

2 Model system

A schematic of the model system is shown in Fig. 1. The system components are grouped into a storage block, a power block, and a heat exchanger block. The main components of the storage block are the reduction and oxidation reactors and the storage tanks for the reduced and oxidized manganese oxide particles. During on-sun operation of the system,

oxidized particles are heated and thermally reduced in the reduction reactor. The energy source for the endothermic reduction reaction is concentrated solar radiation, provided by a heliostat field and a secondary concentrator (not modeled). Oxidized particles are fed to the reduction reactor in a gas flow. A cyclone separator (separator 1) is used to separate the particles from the gas flow after the reduction reactor. The hot reduced particles are stored in the reduced particle storage tank, while the hot gases provide the heat to run the power cycle. During off-sun operation, reduced particles are cooled and re-oxidized to generate hot gases that provide the heat to run the power cycle. Reduced particles are pre-cooled in heat exchanger 3 before they are fed to the oxidation reactor in a gas flow. A cyclone separator (separator 3) is used to separate the particles from the gas flow after the oxidation reactor.

The reduction reaction (Eq. 2) is conducted in inert gas, modeled as nitrogen, while the oxidation reaction (Eq. 3) is conducted in pure oxygen. Each reactor is operated with a closed gas loop. In the inert gas loop over the reduction reactor, oxygen is accumulated, which needs to be continuously removed from the gas loop with a gas-gas separator (separator 2) [7, 8]. The separated oxygen is pressurized with a gas compressor (compressor 2) and stored in a storage tank. During off-sun operation, the stored oxygen is released and expanded via a throttle, and used in the gas loop over the oxidation reactor to compensate for the oxygen consumed by the oxidation reaction.

The power block comprises a topping solar-driven indirectly-heated air Brayton cycle and a bottoming steam Rankine cycle heated by the exhaust heat from the Brayton cycle. The Rankine cycle includes a single-stage reheating process.

The heat exchanger block couples the storage block with the power block. In heat exchanger 1, the hot gas exiting the reduction reactor heats the compressed air from the Brayton cycle during on-sun operation. In heat exchanger 3, the hot particles exiting the reduced particle storage heat the air from the Brayton cycle. The oxidation reactor serves simultaneously as a reactor and heat exchanger, exchanging heat between the oxidizing particle/gas flow and the air from the Brayton cycle.

The power system is designed to operate round-the-clock at a constant power, with 8 hours of on-sun operation and 16 hours of off-sun operation. The particle and gas flow rates entering the reduction reactor (state points N2 and M5 in Fig. 1) are adjusted such that the system generates a constant power output.

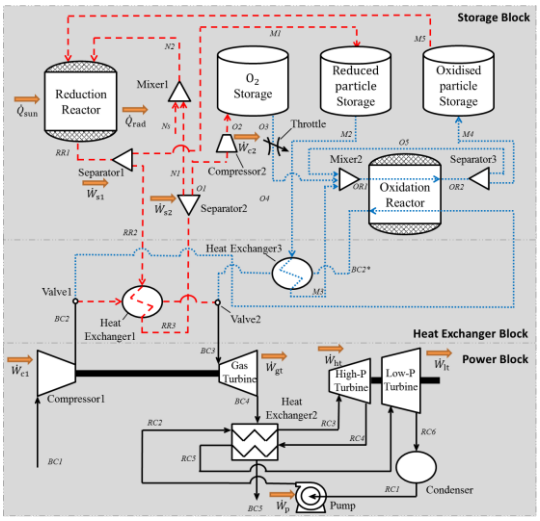

Fig. 1. Schematic of the model system (black solid lines: on- and off-sun operation; red dashed lines: on-sun operation; blue dotted lines: off-sun operation).

3 Thermodynamic model

3.1 Model assumptions

The thermodynamic model of the system shown in Fig. 1 is formulated using the following modeling assumptions. The system is assumed to be at steady state and the air standard assumptions are used. Kinetic and potential energy changes are neglected. The heat loss from the receiver is modeled as black body radiation emission. Heat losses from other system components and connections are neglected. Pressure drop in tubes or heat exchangers are neglected. The thermodynamic effect of oxygen is neglected. System design parameters are listed in Table 2.

Table 2. System design parameters. State points are shown in Fig. 1.

Parameter	Value
Solar power input	100 MW
Solar concentration ratio at the receiver	3000
Direct normal solar irradiation	1000 W/m^{-2}
Brayton cycle compression ratio	10
Efficiency of compressors, turbines, pumps	88%
Efficiency of separators	60% [8, 9]
Pressure at BC1	1 atm
Pressure at BC5	1 atm
Pressure at RC1	9.58 kPa
Pressure at RC2	100 atm [10]
Temperature at BC1	25°C
Temperature at BC3	1580°C
Temperature at RC3 and RC5	565°C
Temperature difference between BC3 and RR2	20°C
Temperature difference between BC5 and RC2	20°C
Temperature of Reduction Reactor	1600°C
Temperature of Oxidation Reactor	750°C
Pressure in solid storage	1 atm
Pressure in gas storage	20 atm

3.2 Model equations

For the reduction and oxidation reactors, the overall steady-state energy balance reduces to:

$$\dot{Q} = \sum_{\mathrm{r}} \dot{n}_{\mathrm{r}} \left(\bar{h}_{\mathrm{f}}^{\mathrm{o}} + \Delta \bar{h} \left(T \right) \right)_{\mathrm{r}} - \sum_{\mathrm{p}} \dot{n}_{\mathrm{p}} \left(\bar{h}_{\mathrm{f}}^{\mathrm{o}} + \Delta \bar{h} \left(T \right) \right)_{\mathrm{p}} \tag{4}$$

where $\dot{Q}$ is the heat rate supplied to the reactor, $\dot{n}$ denotes the molar flow rates into and out of the reactor, $\bar{h}_{\mathrm{f}}^{\mathrm{o}}$ denotes the enthalpy of formation of a substance at reference temperature $T_{\mathrm{ref}} = 298$ K and standard pressure p^{o} = 1.013 bar, and $\Delta \bar{h} \left(T \right)$ denotes the enthalpy change of a substance between temperatures T and T_{ref}.

The reduction reactor is assumed to be a cavity-type radiation receiver that behaves like a black body. The radiative heat loss by the reactor and hence its absorption efficiency depend on the solar concentration ratio, C. The absorption efficiency is given by:

$$\eta_{\mathrm{b}} = 1 - \sigma T_{RR}^{4} / CI \tag{5}$$

where σ is the Stefan-Boltzmann constant, T_{RR} is the reduction reactor temperature, and I is the direct normal irradiation (I = 1 kWm^{-2}).

For the compressors, the feedwater pump, the gas turbine and the two steam turbine stages, and separator 1, the overall energy balance is:

$$\dot{Q} - \dot{W} = \sum_{\text{OUT}} \dot{n}\Delta\bar{h} - \sum_{\text{IN}} \dot{n}\Delta\bar{h} \tag{6}$$

For heat exchangers, the energy balance simplifies to:

$$\dot{n}_{\text{h}}(\bar{h}_{\text{h,in}} - \bar{h}_{\text{h,out}}) = \dot{n}_{\text{c}}(\bar{h}_{\text{c,out}} - \bar{h}_{\text{c,in}}) \tag{7}$$

The total amount of a medium stored in a storage tank is calculated by integrating the mole balance for each single storage medium:

$$n_{\text{net}} = (\dot{n}_{\text{in}} - \dot{n}_{\text{out}})t \tag{8}$$

where n_{net} is the number of moles of storage medium in the storage.

Separators 1 and 3 are modeled as cyclone gas-solid separators, based on the design by Wang et al., 2006 [9]. Separator 1 operates at 1600°C and 1 atm. The gas-solid mixture enters the separator from the side. The gas exits the separator at the top, while the solids exit at the bottom. The pressure drop over the separator is calculated according to the model by Shepheard and Lapple 1939 [11]:

$$\Delta p = 0.003\rho g v_{\text{in}}^2 H_{\text{v}} \tag{9}$$

$$H_{\text{v}} = K d_7 d_8 / d_2^2 \tag{10}$$

where ρ is the density of the gas, g is the gravitational acceleration, v_{in} is the gas velocity at the separator inlet, H_{v} is the inlet gas velocity head, and K is a cyclone configuration and operating condition parameter. Parameters d_2, d_7 and d_8 are dimensions of the separator. The inlet and outlet enthalpies of the gas flow can then be obtained from their temperature and pressure. The electrical pumping power required to operate separator 1 is calculated from Eq. (6). Separator 3 has negligible influence on the system performance due to the relatively small oxygen gas flow rate.

Separator 2 separates O_2 and N_2 in the temperature range of 330–370°C and at a pressure of 1 atm. Ezbiri et al., 2015 [8] showed the feasibility to separate O_2 from N_2 at temperatures of 327 to 627°C. The minimum required energy to separate two gas components in a mixture corresponds to the Gibbs free energy change involved when the two components are mixed. On a molar basis of the component with the smaller molar fraction, x, in the mixture, this yields [12]:

$$\dot{W}_{\text{sp},x} = -RT[(1-x)\ln(1-x) + x\ln x]/x \tag{11}$$

where R and T are the ideal gas constant and the absolute temperature of the mixture, respectively. The actual electrical power required to separate the gas mixture is obtained from:

$$\dot{W}_{\text{sp2}} = \dot{W}_{\text{sp},x} / \eta_{\text{sp2}} \tag{12}$$

where η_{sp2} is the efficiency of separator 2.

The required size of each storage tank is estimated based on the molar flow rate of the material stored in the tank:

$$\phi V = M\dot{n}t_{\text{on}} / \rho \tag{13}$$

where ϕ is the particle volume fraction [13], ρ and M are the mass density and the molar mass of the stored material, respectively, $\dot{n}$ is the charging molar flow rate, and t_{on} is the charging time.

The off-sun operation molar flow rate $\dot{n}_{off}$ is calculated via conservation of mass:

$$\dot{n}_{on} t_{on} = \dot{n}_{off} t_{off} \tag{14}$$

The combined power cycle operates under the same conditions during on-sun and off-sun operation. The net thermal efficiency of the power cycle is calculated as:

$$\eta_{th} = (\dot{W}_{gt} + \dot{W}_{st,H} + \dot{W}_{st,L} - \dot{W}_{cp1} - \dot{W}_{pm}) / \dot{Q}_{he1} \tag{15}$$

where $\dot{W}_{gt}$, $\dot{W}_{st,H}$, $\dot{W}_{st,L}$, $\dot{W}_{cp1}$, $\dot{W}_{pm}$ are the power of gas turbine, high-pressure steam turbine, low-pressure steam turbine, compressor 1 and pump respectively, while $\dot{Q}_{he1}$ is the heat transfer rate in heat exchanger 1.

The overall solar-to-electric energy conversion efficiency of the system is:

$$\eta_{overall} = [(\dot{W}_{gt} + \dot{W}_{st,H} + \dot{W}_{st,L} - \dot{W}_{cp1} - \dot{W}_{pm}) t_{total} - (\dot{W}_{sp1} + \dot{W}_{sp2} + \dot{W}_{cp2}) t_{on}] / (\dot{Q}_{sun} t_{total}) \tag{16}$$

where $\dot{W}_{sp1}$, $\dot{W}_{sp2}$, $\dot{W}_{cp2}$ are the power input into separator 1, separator 2, and compressor 2, respectively, while $\dot{Q}_{sun}$ is the solar power input. Separator 3 only separates a small amount of carrier gas which requires negligible energy input.

3.3 Solution methods

The model equations are solved with Matlab [14]. The thermophysical properties of water and air are obtained from RefProp Mini [15]. Thermochemical data for O_2, N_2, Mn_2O_3 and MnO are obtained from Binnewies and Milke [16].

4 Results

4.1 Power cycle analysis

The following results are calculated using the design parameters listed in Table 2. The off-sun operation duration can be set to 16 hours by changing the ratio of N_2 and Mn_2O_3 molar flow rates (n) at the entrance of the reduction reactor. More N_2 means more solar energy is used directly for on-sun operation, while more Mn_2O_3 means more energy is stored for off-sun operation. Numerical modelling shows that with n = 2.96, the off-sun operation duration is 16 hours.

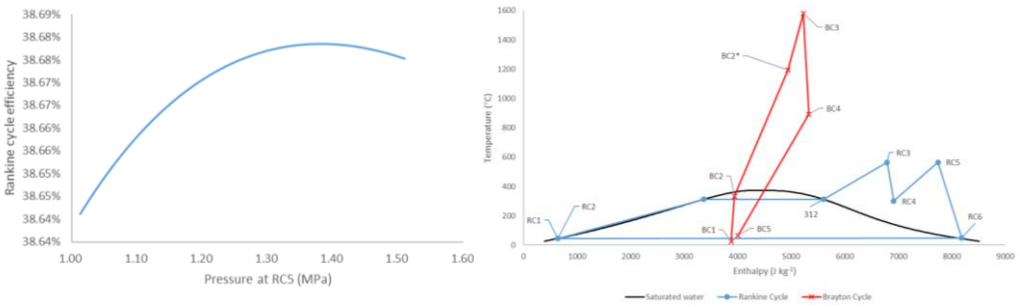

(a) (b)

Fig. 3. (a) The effect of p_{RC5} on Rankine cycle efficiency; (b) *T-s* diagram of the combined cycle for the power cycles (BC2* is only for off-sun operation).

The Rankine cycle has a single-stage reheating process. The pressure at the low-pressure steam turbine outlet, P_{RC5}, can be optimized numerically for maximum cycle efficiency (Fig 3a). The resulting maximum Rankine cycle efficiency of 38.68% is obtained when p_{RC5} = 1.38 MPa.

The *T-s* diagram for the combined power cycle is shown in Fig. 3b. During off-sun operation, the Brayton cycle is heated in two steps, which is the only difference from on-sun operation. The flow rates of the combined cycle working fluids are the same for on-sun and off-sun, while the flow rates of the thermal storage materials are different.

4.2 Efficiencies and storage tank sizes

Fig. 4 shows energy balance and work allocation of the system over a 24-hour period. The total daily solar energy input to the system is 800 MWh. The largest energy loss of 186.08 MWh/day is due to blackbody radiation losses from the solar receiver, which operates with an absorption efficiency, η_b, of 76.74%. Additional main energy losses are due to the power input to compressors and separators. Compressors 1 and 2 and separator 2 require the largest amounts of work, amounting to 151.92 MWh/day, 19.92 MWh, and 18.88 MWh, respectively. The daily net work output is 330.32 MWh. The work requirement of the feedwater pump of the Rankine cycle is negligible. The predicted thermodynamic efficiency of the combined cycle η_{th}, is 60.04%. The predicted overall solar-to-electric energy conversion efficiency, $\eta_{overall}$, is 41.30%.

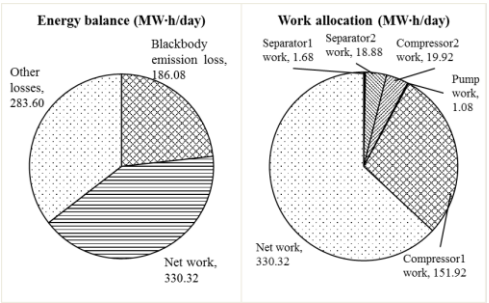

Fig. 4. Energy balance and work allocation of the system.

The required volume of the O_2 storage is 1.55×10^4 m^3 at a storage pressure of 20 atm, while the volume of reduced particle storage (MnO) and oxidised particle storage (Mn_2O_3) are 2.83×10^2 m^3 and 3.81×10^2 m^3, respectively. The MnO and Mn_2O_3 storage volumes are significantly smaller than those of a 120 MW molten salt power plant designed for round-the-clock operation, which are around 1.8×10^3 m^3 each [17]. On the other hand, the required size of the O_2 storage tank is one order of magnitude larger and may prove to be uneconomically large.

5 Summary and conclusions

In this paper, a thermodynamic model has been presented for a solar thermal power plant with a combined power cycle and high-temperature thermochemical energy storage system based on manganese oxide redox cycling. The gas-solid molar flow ratio at the reduction reactor inlet was determined for steady round-the-clock operation with 8 hours of on-sun and 16 hours of off-sun operation. The Rankine cycle reheating pressure was optimized for maximum power cycle efficiency. The overall solar-to-electric energy conversion efficiency and the net power block efficiency were determined to be 41.3% and 60.0%, respectively. Main energy losses in the system are due to blackbody emission by the solar reactor, and power demands by the pumps, compressors, and separators in the system, in addition to the heat rejected by the power cycle. For a system with 100 MW solar energy input, the volumes of reduced and oxidized particle storage tanks are estimated to be approx. 5–6 times smaller than those of a comparable molten salt-based plant [17]. On the other hand, the required O_2 storage volume of 1.51×10^4 m^3 is comparatively large.

This paper establishes the methodology to determine the efficiency of solar combined cycle power plants with thermochemical energy storage and provides an estimation of the theoretical system efficiency for an exemplary plant design. To obtain more accurate predictions of the annual plant efficiency, year-round simulations for a particular location need to be conducted and the component models need to be refined to take into account additional irreversibilities, e.g. due to flow friction, additional heat losses, incomplete chemical reactions, part-load efficiencies, etc. It is also recommendable to study different system parameters, such as the solar concentration ratio and the reduction temperature, and to consider alternative system configurations, including the possibility of operating both chemical reactors with atmospheric air, which would eliminate the potential challenges associated with the storage of gaseous oxygen and gas-gas separation.

Financial support by the Australian Renewable Energy Agency, grant no. 2014/RND005, is gratefully acknowledged.

References

1. International Energy Agency, *Technology Roadmap Solar Thermal Electricity* (2014)
2. A. Kribus, R. Zaibel, D. Carey, A. Segal, J. Karni, Sol. Energy **62**,121 (1998)
3. S. Baykal, P. Rufli, R. Bolliger, F. Fusaro, H. Kujawski, *ASME Turbo Expo* (2016)
4. Siemens, Siemens Gas Turbines, *Siemens AG*, (2017). Available: http://www.energy.siemens.com/hq/en/fossil-power-generation/gas-turbines
5. B. Ehrhart, E. Coker, N. Siegel, A. Weimer, Energy Procedia **49**, 762 (2014)
6. C. Bale, E. Bélisle, P. Chartrand, S. Decterov, G. Eriksson, K. Hack, I. Jung, Y. Kang, J. Melançon, A. Pelton, C. Robelin, S. Petersen, Calphad **33**, 295 (2009)

7. D. Meixner, D. Brengel, B. Henderson, J. Abrardo, M. Wilson, D. Taylor, R. Cutler, J. Electrochem. Soc. **9**, D132 (2002)
8. M. Ezbiri, K. Allen, M. Gàlvez, R. Michalsky, A. Steinfeld, ChemSusChem. **8**, 1966 (2015)
9. B. Wang, D. Xu, K. Chu, A. Yu, Appl. Math. Model. **30**, 1326 (2006)
10. Siemens AG, Industrial Steam Turbines, Duisburg (2013)
11. C. Shepherd, C. Lapple, *Air Pollution Control: A Design Approach. In Cyclones* (1939)
12. M. Hänchen, A. Stiel, Z. Jovanovic, A. Steinfeld, Ind. Eng. Chem. Res. **51**, 7013 (2012)
13. D. Kunii, O. Levenspiel, *Fluidization Engineering* (1991)
14. The MathWorks, Inc., *MATLAB and Statistics Toolbox Release 2015b* (2015)
15. E. Lemmon, M. Huber, M. McLinden, *Reference Fluid Thermodynamic and Transport Properties (REFPROP MINI)* (2015)
16. M. Binnewies, E. Milke, *Thermochemical Data of Elements and Compounds* (2002)
17. J.I. Burgaleta, S. Arias, D. Ramirez, *Proceedings of 2011 SolarPACES, Conference* (2011)